

Fig. 2. Differential cross section when incident wave is polarized along  $z$  axis.

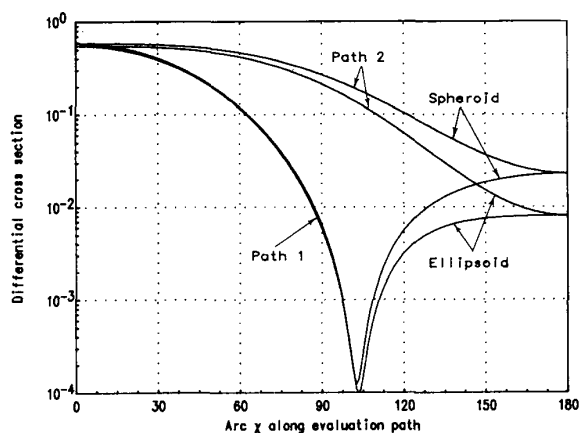


Fig. 3. Differential cross section when incident wave is polarized along  $y$  axis.

except the incident plane wave is now polarized along the  $y$  axis. As before, the two scatterers appear quite similar in differential cross section when the angle is less than a certain amount, approximately  $105^\circ$  in this case, but strong differences appear beyond this value.

## VI. SUMMARY

The extended boundary condition method has been summarized and the dielectric ellipsoid scattering problem formulated in the resonant range. It is thus possible to consider scattering properties of a broader class of targets than those previously found in the literature, specifically those that lack rotational symmetry. Calculated results have been included, and the importance of this extension beyond the rotationally symmetric scatterer is emphasized in terms of a comparison between a dielectric ellipsoid and a spheroid having approximately the same total volume. The importance of differences in the surface and internal propagation paths provided by the two scatterers is evident. More specific interpretations of the differences are difficult to achieve in the resonance region. For example large particle approximations can explain some of the results; small particle approximations interpret others. The inconsistencies appear to be inherent to this region and will be a topic for further study.

The work reported here can provide a basis for further extension to

multiple body scattering and also shows promise for categorizing some irregular dielectric shapes in terms of their inclusion in best-fit ellipsoids. This latter aspect is being pursued, as is the immersion of the scatterer in lossy media where it may be especially appropriate for target classification and identification.

## ACKNOWLEDGMENT

All values shown in Figs. 2 and 3 were calculated on the Cray X-MP/48 at the San Diego Supercomputer Center.

## REFERENCES

- [1] P. C. Waterman, "Symmetry, unitarity, and geometry in electromagnetic scattering," *Phys. Rev. D*, vol. 3, no. 4, pp. 825-839, 1971.
- [2] P. Barber and C. Yeh, "Scattering of electromagnetic waves by arbitrary shaped dielectric bodies," *Appl. Opt.*, vol. 14, no. 12, pp. 2864-2872, 1975.
- [3] C. Yeh, S. Colak, and P. Barber, "Scattering of sharply focused beams by arbitrarily shaped dielectric particles: an exact solution," *Appl. Opt.*, vol. 21, no. 24, pp. 4426-4433, 1982.
- [4] P. W. Barber, J. F. Owen, and R. K. Chang, "Resonant scattering for characterization of axisymmetric dielectric objects," *IEEE Trans. Antennas Propagat.*, vol. 30, no. 2, pp. 168-172, 1982.
- [5] A. R. Holt, "The scattering of single hydrometeors," *Radio Sci.*, vol. 17, no. 5, pp. 929-945, 1982.
- [6] —, "Electromagnetic wave scattering by spheroids: A comparison of experimental and theoretical results," *IEEE Trans. Antennas Propagat.*, vol. 30, no. 4, pp. 758-760, 1982.
- [7] A. Mugnai and W. Wiscombe, "Scattering from nonspherical Tschebyscheff particles. 1: Cross sections, single scattering albedo, asymmetry factor and backscattered fraction," *Appl. Opt.*, vol. 25, no. 7, pp. 1235-1244, 1986.
- [8] G. Kristensson and S. Ström, "Electromagnetic scattering from geophysical targets by means of the  $T$  matrix approach: A review of some recent results," *Radio Sci.*, vol. 17, no. 5, pp. 903-912, 1982.
- [9] A. Karlsson and G. Kristensson, "Electromagnetic scattering from subterranean obstacles in a stratified ground," *Radio Sci.*, vol. 18, no. 3, pp. 345-356, 1983.
- [10] L. Tsang, J. A. Kong, and R. T. Shin, *Theory of Microwave Remote Sensing*. New York: Wiley, 1985, pp. 168-186.
- [11] M. Abramowitz and I. E. Stegun, *Handbook of Mathematical Functions*. Nat. Bur. Standards, 1972, p. 887.

## Scattering from the Perfectly Conducting Cube

MARC G. COTE, MEMBER, IEEE, MARGARET B. WOODWORTH, MEMBER, IEEE AND ARTHUR D. YAGHJIAN, SENIOR MEMBER, IEEE

**Abstract**—The scattering cross sections in the  $E$ -plane,  $H$ -plane, and  $45^\circ$ -plane of the perfectly conducting cube illuminated broadside by an incident plane wave are computed using both a uniform high-frequency diffraction solution and magnetic-field integral equations. The computed cross sections are compared with measured cross sections for cube perimeters of 3, 6, 12, and 20 wavelengths. The total scattering cross section versus the perimeter of the cube is also computed and compared to that of the sphere.

Manuscript received August 20, 1987; revised February 1, 1988.

M. G. Cote and A. D. Yaghjian are with the Rome Air Development Center, Hanscom Air Force Base, Bedford, MA 01731.

M. B. Woodworth is with the Arcon Corporation, 260 Bear Hill Road, Waltham, MA 02154.

IEEE Log Number 8821493.

## I. INTRODUCTION

In a previous paper [1],<sup>1</sup> we determined the backscattered fields of a plane wave incident broadside upon the perfectly conducting cube shown in Fig. 1. In particular, the broadside radar cross section (RCS) was predicted from the low-frequency "Rayleigh region" to arbitrarily high frequencies, and the predicted RCS was compared with measurements taken over a cube side length ranging from 0.15 to 4 wavelengths (see Fig. 2). From the low-frequency Rayleigh region through intermediate frequencies above resonance, the predicted RCS of Fig. 2 was obtained with the augmented magnetic-field integral equation (AMFIE) [1], [2]. From the resonance region to arbitrarily high frequencies, the predicted RCS of Fig. 2 was determined from an "enhanced" high-frequency diffraction solution [1]. Agreement to within about  $\pm 1$  dB between these two very different low and high-frequency solutions over their common intermediate range of frequencies, and with experimental data, has allowed us to use these scattered fields of the cube (a full-bodied three-dimensional scatterer with edges and corners) as a benchmark solution to evaluate the range of validity of general numerical codes that compute scattering.

In this communication we present the predicted and measured  $E$ -plane,  $H$ -plane, and  $45^\circ$ -plane scattered fields from the perfectly conducting cube for broadside plane-wave incidence. These bistatic scattered fields were not included in the previous paper [1] because a uniform high-frequency solution had not been obtained except for the backscattering direction, and an automated bistatic RCS measurement system [3] for determining scattering cross section versus angle had not been completed.

## II. THE UNIFORM HIGH-FREQUENCY DIFFRACTION SOLUTION

The scattering cross sections for various cube sizes are shown in Figs. 3-6. The solid lines of Figs. 3-5 are computed from the same AMFIE solution used in [1], but with the computer program rewritten for direct-access storage of the impedance matrix to allow the application of the AMFIE to electrically larger cubes [4]. The solid lines for the electrically largest cube (Fig. 6) are computed from the "dual-surface" magnetic-field integral equation [4], which is better conditioned than the AMFIE<sup>2</sup> for a faster matrix solution by the conjugate gradient method. Both integral equations were approximated numerically by assuming the current was constant over each of the rectangular patches that divided the surface of the cube. The value of the Green's function over each patch was taken as a constant equal to its value at the center of the patch. The integral equation was applied at the center of each patch, and  $xy$  symmetry was used to reduce the number of unknowns by a factor of four.

The dashed lines are computed from a uniform high-frequency solution (1) that gives continuous scattered far fields in all directions for broadside plane-wave incidence. This uniform high-frequency solution was derived by assuming that the front and back edges of the cube were truncated portions of infinite right-angled wedges. Distortion of the truncated wedge currents near the corners of the cube and near the four edges parallel to the  $z$  axis were neglected. To a first approximation (singly diffracted fields), the fields impinging

<sup>1</sup> In [1], the contribution  $\tilde{I}^x$  in the paragraph containing equation (14) was evaluated incorrectly. A correct evaluation shows that  $\tilde{I}^x$  is negligible compared to  $\tilde{I}^{y0}$ , and thus the  $\tilde{F}_x$  term in (15) should be set equal to zero. This change affects the curve of Fig. 2 in [1] imperceptibly except for raising the resonance null (near  $4s/\lambda = 1.5$ ) to  $-15$  dB.

<sup>2</sup> The AMFIE produces an overdetermined set of equations that is solved by multiplying by the Hermitian conjugate of the coefficient matrix. This Hermitian conjugate multiplication yields a matrix with higher condition number than that of the even-determined dual-surface MFIE. Thus AMFIE requires a greater number of iterations than the dual surface MFIE to achieve the same residual error with the conjugate gradient method.

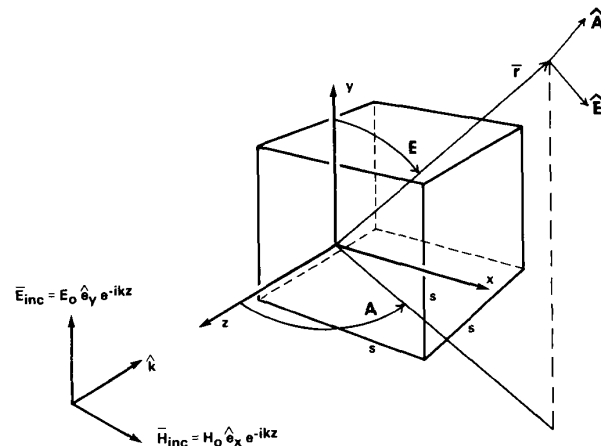


Fig. 1. Perfectly conducting cube with side length  $s$  and broadside plane-wave incidence.

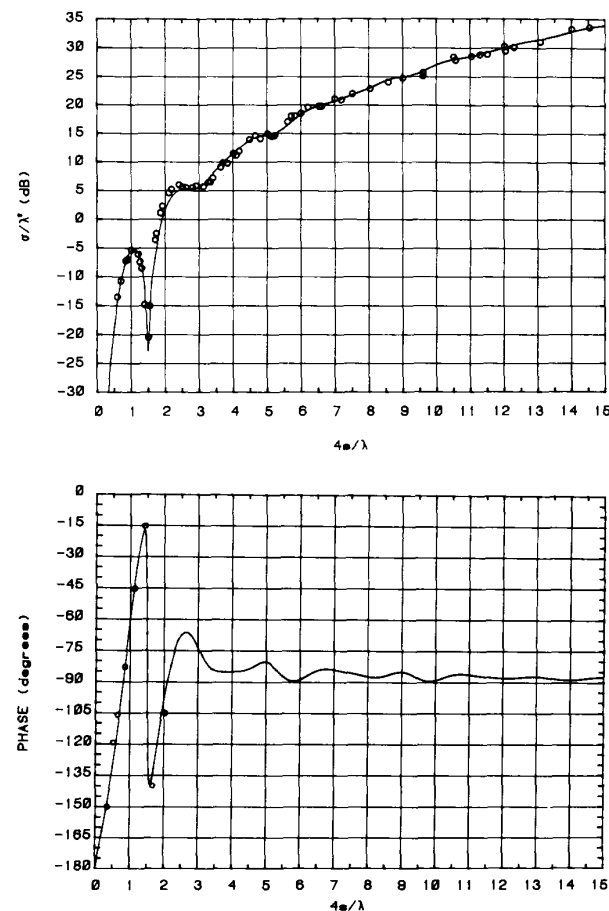


Fig. 2. Top: broadside RCS of perfectly conducting cube. Bottom: Phase of backscattered far magnetic field referenced to incident magnetic field on front face of cube; — predicted, ○○○○○ measured.

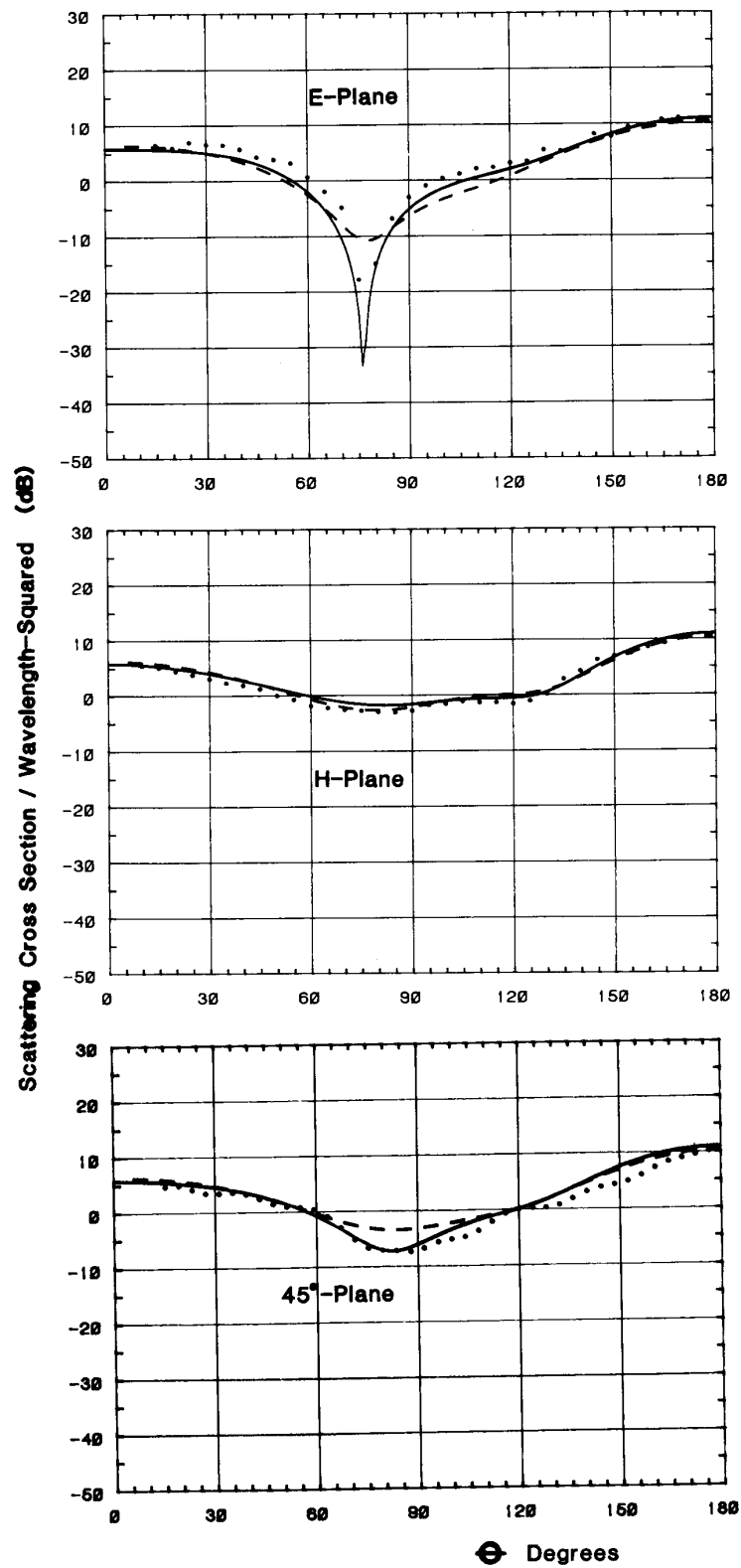


Fig. 3. Scattering from cube with perimeter  $4s = 3\lambda$ ; — AMFIE, ---- high-frequency solution, ○○○○○ measured.

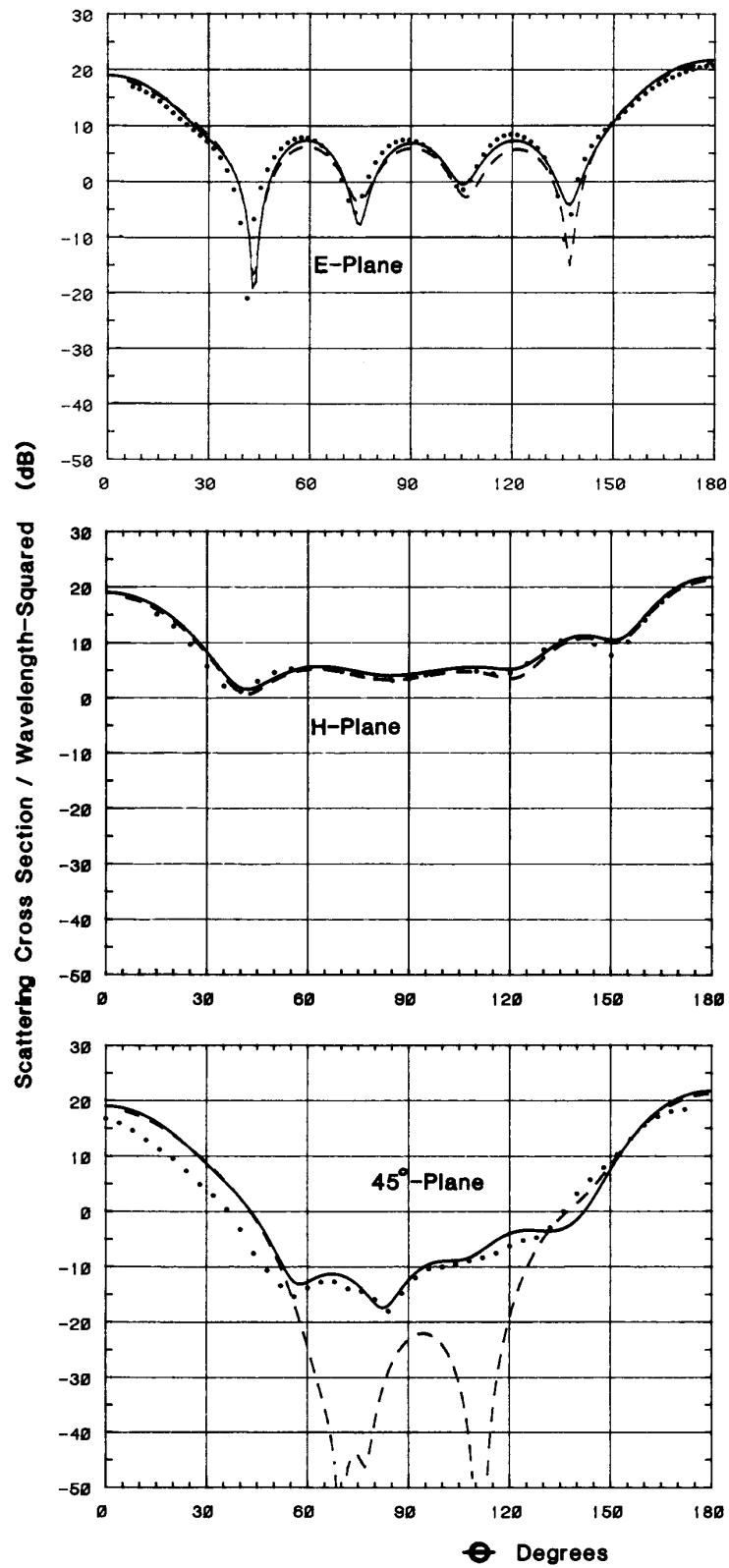


Fig. 4. Scattering from cube with perimeter  $4s = 6\lambda$ ; — AMFIE, ---- high-frequency solution, ○○○○○ measured.

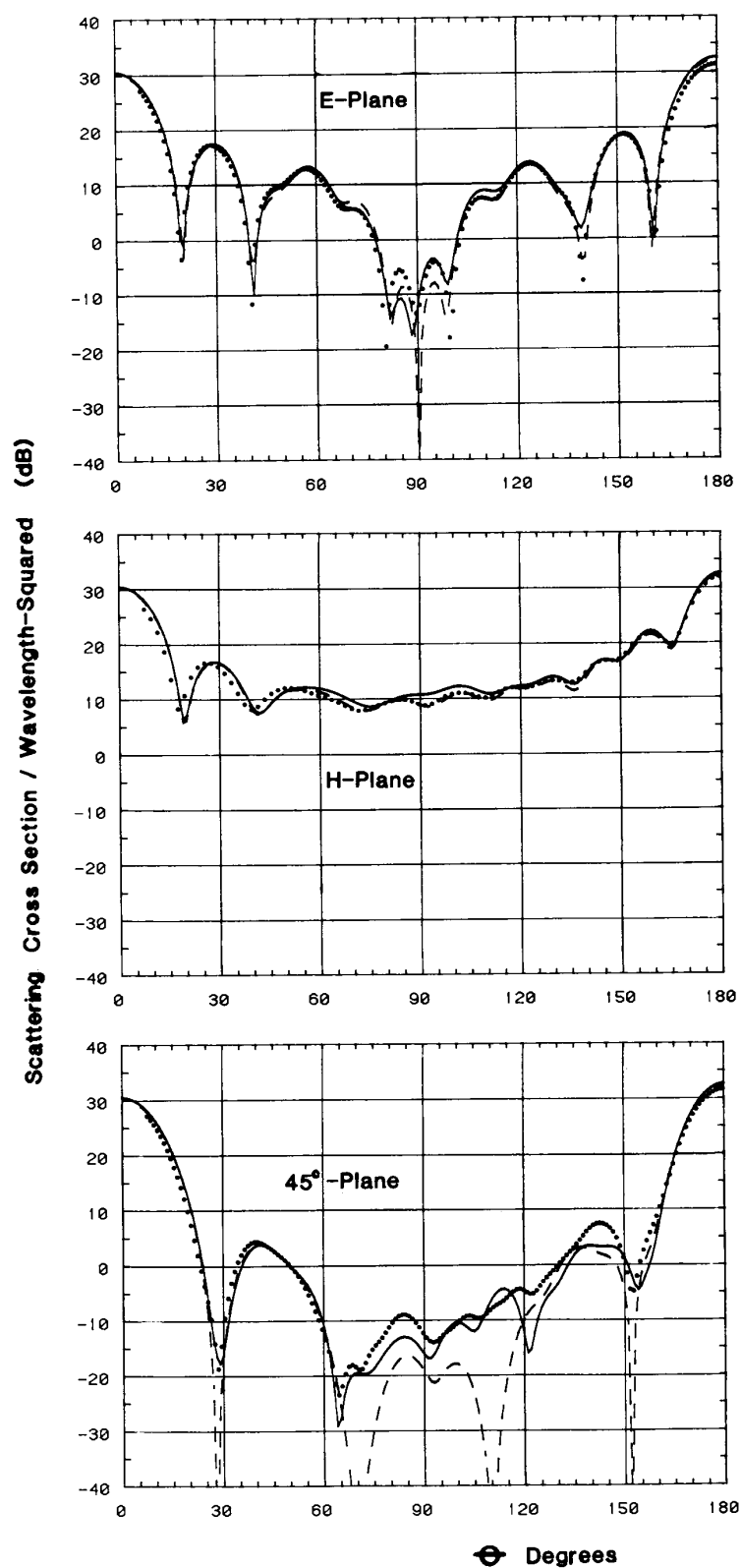


Fig. 5. Scattering from cube with perimeter  $4s = 12\lambda$ ; — AMFIE, ---- high-frequency solution, ○○○○○ measured.

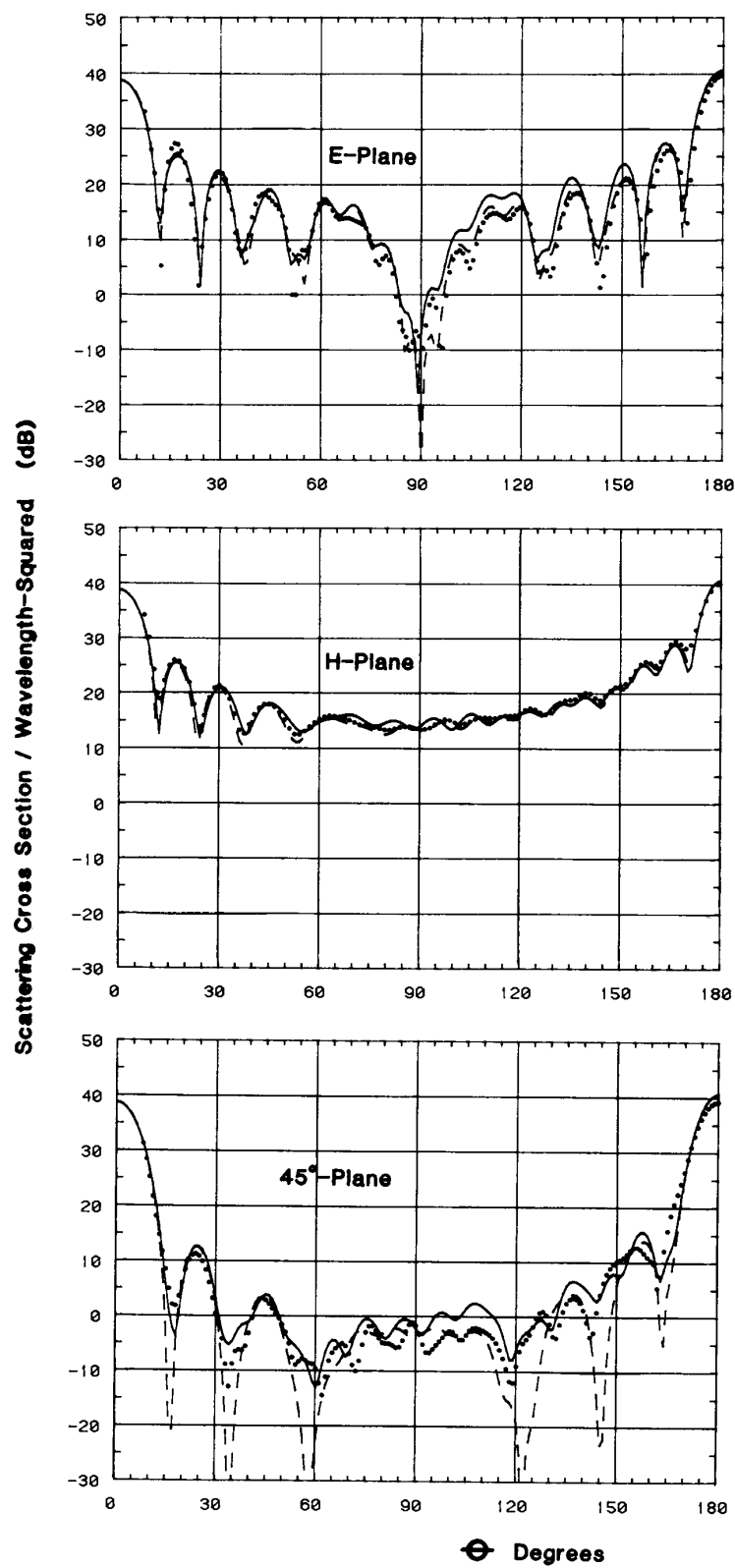


Fig. 6. Scattering from cube with perimeter  $4s = 20\lambda$ ; — dual-surface MFIE, ---- high-frequency solution, oooooo measured.

upon the four front wedges are merely the incident plane-wave fields. Similarly, the fields impinging on the top and bottom back wedges ( $y = \pm s/2, z = -s$ ) are, to a first approximation, the grazing incident plane-wave fields [5], or alternatively, 1/2 the total (incident plus reflected) fields [10]. The fields impinging on the left and right back wedges ( $x = \pm s/2, z = -s$ ) are negligible to a first approximation since the incident  $E$ -field is parallel to the sides of the cube and thus produces currents that decay asymptotically from the corresponding front edges [5].

These fields impinging on the front and back edges of the cube induce currents on all six faces of the cube that are given, to a first approximation, by the currents on the right-angled wedges associated with the illuminated front and back edges. Closed-form expressions for the far fields radiated by an infinitesimal increment of current on each separate face of a wedge illuminated by a plane wave can be derived by combining the results of Michaeli's two papers [6] and [7]. Thus it is a straightforward (though tedious) procedure to add these incremental far fields integrated a distance  $s$  along the illuminated front and back edges of the cube to obtain the following expression for the scattered far magnetic field:

$$\vec{H}_{sc} = \frac{H_0 k s}{2\pi} \frac{e^{ikr}}{kr} (\vec{h}^F + \vec{h}^B + \vec{h}^{TB} + \vec{h}^{LR}). \quad (1)$$

The functions  $\vec{h}^F$ ,  $\vec{h}^B$ ,  $\vec{h}^{TB}$ , and  $\vec{h}^{LR}$  are the normalized scattered magnetic far fields radiated by the currents on the front face, the back face, the top and bottom faces ( $y = \pm s/2$ ), and the left and right faces ( $x = \pm s/2$ ) of the cube, respectively. These functions are given explicitly by

$$\vec{h}^F = \hat{A} \left\{ \frac{\sin E}{\sqrt{3}} \frac{\sin \left( \frac{ks}{2} \cos E \right)}{\frac{ks}{2} \cos E} \right. \\ \cdot \left( \frac{e^{i(ks/2) \sin E \sin A}}{C(-\cos^{-1}(\sin E \sin A))} \right. \\ \left. + \frac{e^{-i(ks/2) \sin E \sin A}}{C(\cos^{-1}(\sin E \sin A) - \pi)} \right. \\ \left. + \sqrt{3} i k s \frac{\sin \left( \frac{ks}{2} \sin E \sin A \right)}{\frac{ks}{2} \sin E \sin A} \right) \\ \left. + \frac{\sin \left( \frac{ks}{2} \sin E \sin A \right)}{\frac{ks}{2} \sin E \sin A} \left[ \left( \frac{2}{3} \sin \frac{2}{3} (\pi - E) \right) \right. \right. \\ \left. \cdot \frac{e^{i(ks/2) \cos E}}{C(-E)} + \frac{2}{3} \sin \frac{2}{3} E \frac{e^{-i(ks/2) \cos E}}{C(E - \pi)} \right) \\ \left. + \frac{\sin E}{\sqrt{3}} \left( e^{i(ks/2) \cos E} G(-\cos E) \right. \right. \\ \left. \left. + e^{-i(ks/2) \cos E} G(\cos E) \right) \right] \Bigg\}$$

$$\vec{h}^B = -\hat{A} \frac{\sin \left( \frac{ks}{2} \sin E \sin A \right)}{\frac{ks}{2} \sin E \sin A} e^{iks(1 + \sin E \cos A)} \\ \cdot \left[ \frac{2}{3} \sin \frac{2}{3} (\pi - E) \frac{e^{i(ks/2) \cos E}}{2C(-E) + 3} \right. \\ \left. + \frac{2}{3} \sin \frac{2}{3} E \frac{e^{-i(ks/2) \cos E}}{2C(E - \pi) + 3} - \frac{\sin E}{\sqrt{3}} \right. \\ \left. \cdot \left( e^{i(ks/2) \cos E} G(-\cos E) + e^{-i(ks/2) \cos E} G(\cos E) \right) \right] \\ \vec{h}^{TB} = (\hat{A} \cos E \cos A + \hat{E} \sin A) \\ \cdot \frac{\sin \left( \frac{ks}{2} \sin E \sin A \right)}{\frac{ks}{2} \sin E \sin A} \frac{4i \sin \left( \frac{ks}{2} \cos E \right)}{3\sqrt{1 - \sin^2 E \cos^2 A}} \\ \cdot \left[ \frac{\sin \frac{2}{3} (\pi + \sin^{-1}(\sin E \cos A))}{C(\sin^{-1}(\sin E \cos A))} \right. \\ \left. \cdot \frac{e^{iks(1 + \sin E \cos A)} \sin \frac{2}{3} (\pi - \cos^{-1}(\sin E \cos A))}{2C(-\cos^{-1}(\sin E \cos A)) - 1} \right] \\ \vec{h}^{LR} = -\hat{A} 2 \sin E \cos \left( \frac{ks}{2} \sin E \sin A \right) \\ \cdot \frac{\sin \left( \frac{ks}{2} \cos E \right)}{\frac{ks}{2} \cos E} \left[ \frac{1}{\sqrt{3} C(\sin^{-1}(\sin E \cos A))} \right. \\ \left. + G(\sin E \cos A) \right]$$

with

$$C(x) \equiv \cos \frac{2}{3} (\pi + x) - \frac{1}{2}$$

$$G(x) \equiv \frac{1 - \exp(-i\pi/4) F(ks(1+x))/\sqrt{\pi}}{\sqrt{2}(1+x)}$$

and

$$F(x) \equiv \int_0^x \frac{e^{it}}{\sqrt{t}} dt.$$

In these equations,  $s$  denotes the side length of the cube, and  $k = 2\pi/\lambda$  is the propagation constant for a free-space wavelength  $\lambda$ .

The azimuth and elevation angles  $A$  and  $E$  and their corresponding unit vectors along the direction of scattering  $\vec{r}$  are defined in Fig. 1. The angles  $A$  and  $E$  range from 0 to  $2\pi$  and 0 to  $\pi$ , respectively, and are related to the conventional spherical angles  $\theta$  and  $\phi$  (measured from the  $z$  and  $x$  axes, respectively, in Fig. 1) by the simple expressions

$$\cos E = \sin \theta \sin \phi \quad (2a)$$

$$\cos A = \frac{\cos \theta}{\sqrt{1 - \sin^2 \theta \sin^2 \phi}}. \quad (2b)$$

The  $G$  functions that contain the Fresnel integrals  $F$  arise from the termination of the  $H$ -wave induced currents that emanate from the top

and bottom edges across the front and back faces of the cube, and from the termination of the  $E$ -wave induced currents that emanate from the left and right front edges along the sides of the cube. Both these currents decay asymptotically as the square root of the distance from their respective edges [5], and thus produce doubly diffracted fields, upon termination at a distance  $s$ , that involve Fresnel integral functions. If these currents are not terminated, the scattered far fields in the  $\pm y$  directions become discontinuous (across the  $H$ -wave current sheets of the extended wedge faces), and the scattered far fields in the  $-z$  direction become infinite (along the extended wedge faces with a grazing  $E$ -wave). (The  $H$ -wave currents along the top and bottom faces of the cube are in opposite directions and thus do not produce discontinuities in the  $\pm z$  directions.)

In the backscatter direction ( $A = 0$ ,  $E = \pi/2$ ), the scattered far field (1) reduces to

$$H_{SC}(A=0, E=\pi/2) = \hat{x} \frac{H_0 k s e^{ikz}}{2\pi k z} \left[ -iks + \frac{2}{3\sqrt{3}} (2 - e^{2iks}) + \frac{2G(0)}{\sqrt{3}} (1 + e^{2iks}) - 2G(1) \right]. \quad (3)$$

The first term on the right side of (3) is the physical optics backscattered far field and checks with the physical optics term of [1, eq. (16)]. The second term in (3) represents the singly diffracted backscattered far fields, which also agree with the singly diffracted far fields of [1, eq. (16)] when  $ks$  is large so that  $F'_0$  in [1, eq. (16)] approaches unity. The  $G$  terms in (3) are the doubly diffracted backscattered far fields excited by terminating the decaying currents on the front, back, left, and right faces of the cube, as mentioned before. They do not agree perfectly, even for large  $ks$ , with the doubly diffracted fields of [1, eq. (16)] because in [1] the doubly diffracted fields were determined more accurately in the backscatter direction using the wedge diffraction coefficients. In this communication we merely terminated the tails of the currents to obtain, by as simple a method as possible, a uniform high-frequency solution free of discontinuities over the complete  $4\pi$  steradians. Michaeli [8] used a similar truncation procedure to obtain continuous scattered fields from polygonal surfaces.

### III. DISCUSSION OF NUMERICAL AND EXPERIMENTAL RESULTS

In Figs. 3–6 we see that the magnetic-field integral equation solutions [1], [4], the uniform high-frequency diffraction solution (1), and the measured data [3] all agree reasonably well with the exception of the high-frequency solution in the central portion of the  $\phi = 45^\circ$  planes. The far fields in this central region of the diagonal planes are determined to a large extent by diffraction from the corners of the cube. Since our high-frequency solution simply truncates the wedge currents at the corners of the cube and neglects higher order distortion of the current near the corners, it fails to predict accurate far fields in the central region of the diagonal planes (where asymptotically there are only endpoint, corner contributions from the edges). The failure of the high-frequency solution in the central region of the diagonal planes of the cube emphasizes the need for corner diffracted fields determined more accurately than the implicit “physical optics” corner diffracted fields [11], [12] produced simply by truncating the wedge currents.

The measured scattering cross sections for cube sizes of  $4s/\lambda = 3$ , 6, and 12 confirm that the AMFIE solution predicts reliable far fields in the diagonal planes as well as in the  $E$ - and  $H$ -planes, using as few as five patches per wavelength (25 per square wavelength). The numerical solution of the dual-surface integral equation [4], although not shown in Figs. 3–5, agreed closely with the AMFIE solution. Fig. 6 compares the dual-surface integral equation and high-

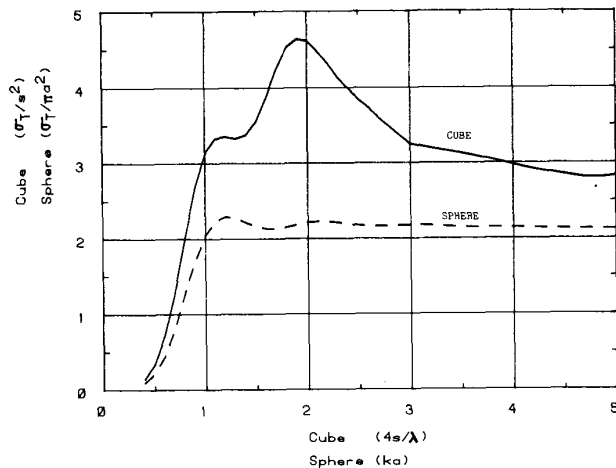


Fig. 7. Normalized total scattering cross section versus circumference (in wavelengths) of cube and sphere.

frequency solution with measured data for the largest cube size of  $4s/\lambda = 20$ . The  $1728 \times 1728$  complex matrix of the dual-surface integral equation for this largest cube was solved with 117 iterations using the conjugate gradient method [9] in 84 min of CPU time on the Vax 8650. The initial value taken for the solution vector in the conjugate gradient iterative scheme was zero, and the iterations were terminated when the ratio of the magnitude of the residual vector to the magnitude of the source vector became less than  $10^{-6}$ .

Although the computer time on the Vax 8650 required to solve the surface integral equations becomes considerable for cubes much larger than several wavelengths on a side, the uniform high-frequency solution (1) takes an insignificant amount of computer time to yield the far fields of cubes hundreds of wavelengths across. Moreover, Fig. 3 shows that the high-frequency solution gives fairly reliable  $E$ - and  $H$ -plane cross sections for cubes as small as three quarters of a wavelength on a side. Thus we find that, for the  $E$ - and  $H$ -planes, the high-frequency solution (1) is an especially convenient and useful solution for scattered fields from frequencies just above resonance to arbitrarily high frequencies.

In all the Figs. 3–6, one sees that the back and forward lobes of the far-field patterns are dominated by the radiation from the physical optics current on the front faces of the cubes. The forward lobes are slightly higher than the backscattered lobes because the currents excited along the grazing faces of the cubes reinforce the physical optics fields in the forward direction. Also, the rectangular symmetry of the cube under the plane-wave illumination shown in Fig. 1 demands that the scattered  $H$ -field in both the  $E$ - and  $H$ -planes has only an azimuthal component, as (1) confirms. However, both components of the far field contribute to the scattering cross section in the  $45^\circ$ -planes.

Fig. 7 compares the normalized total scattering cross sections versus perimeter (in wavelengths) of the cube and sphere. The total scattering cross section of the sphere was computed from the exact eigenfunction solution; the total scattering cross section of the cube was computed from the magnetic-field integral equation augmented above  $4s/\lambda = 2.8$  to avoid the spurious resonances. The total scattering cross section of the cube, unlike that of the sphere, reaches a resonant value at  $4s/\lambda \approx 2$  of about four and a half times the physical cross section.

Although the scattering patterns shown in Figs. 3–6 are excited by a plane-wave incident broadside upon the front face of the cube, the magnetic-field integral equation solutions can easily accommodate plane-wave illumination from an arbitrary direction, or illumination



by an incident field other than a plane wave. However, the uniform high-frequency solution (1) is valid only for broadside plane-wave incidence.

#### ACKNOWLEDGMENT

The authors are indebted to James L. Schmitz and Ernest J. Yasso for their help in performing the bistatic scattering cross section measurements.

#### REFERENCES

- [1] A. D. Yaghjian and R. V. McGahan, "Broadside radar cross section of the perfectly conducting cube," *IEEE Trans. Antennas Propagat.*, vol. AP-33, pp. 321-329, Mar. 1985.
- [2] A. D. Yaghjian, "Augmented electric- and magnetic-field integral equations," *Radio Sci.*, vol. 16, pp. 987-1001, Nov.-Dec. 1981.
- [3] M. G. Cote, "A spatial filtering technique for removing phase errors in automated bistatic scattering measurements," in *Digest Nat. Radio Science Meeting*, Boulder, CO, Jan. 1988, p. 73.
- [4] A. R. Tobin, A. D. Yaghjian, and M. M. Bell, "Surface integral equations for multi-wavelength, arbitrarily shaped, perfectly conducting bodies," in *Digest Nat. Radio Science Meeting*, Boulder, CO, Jan. 1987, p. 9.
- [5] J. J. Bowman, T. B. A. Senior, and P. L. E. Uslenghi, *Electromagnetic and Acoustic Scattering by Simple Shapes*. Amsterdam: North-Holland, 1969, ch. 6.
- [6] A. Michaeli, "Equivalent edge currents for arbitrary aspects of observation," *IEEE Trans. Antennas Propagat.*, vol. AP-32, pp. 252-258, Mar. 1984.
- [7] —, "Contribution of a single face to the wedge diffracted field," *IEEE Trans. Antennas Propagat.*, vol. AP-33, pp. 221-223, Feb. 1985.
- [8] —, "Equivalent currents for second-order diffraction by edges of perfectly conducting polygonal surfaces," *IEEE Trans. Antennas Propagat.*, vol. AP-35, pp. 183-190, Feb. 1987.
- [9] T. K. Sarkar and E. Arvas, "On a class of finite step iterative methods (conjugate directions) for the solution of an operator equation arising in electromagnetics," *IEEE Trans. Antennas Propagat.*, vol. AP-33, pp. 1058-1066, Oct. 1985.
- [10] R. G. Kouyoumjian, "The geometrical theory of diffraction and its application," in *Numerical and Asymptotic Techniques in Electromagnetics, Topics in Applied Physics*, vol. 3, R. Mittra, Ed. New York: Springer-Verlag, 1975, p. 180.
- [11] F. A. Sikta, W. D. Burnside, T. Chu, and L. Peters, Jr., "First order equivalent current and corner diffraction scattering from flat plate structures," *IEEE Trans. Antennas Propagat.*, vol. AP-31, pp. 584-589, July 1983.
- [12] A. C. Ludwig, "Backscattering from a cube," *Appl. Computational Electromagn. Soc. J., Newsletter*, vol. 2, pp. 55-74, Fall 1987.

### An Application of the WKJB Technique to the On-Surface Radiation Condition

THOMAS G. MOORE, STUDENT MEMBER, IEEE,  
GREGORY A. KRIEGSMANN, AND  
ALLEN TAFLOVE, SENIOR MEMBER, IEEE

**Abstract**—The on-surface radiation condition (OSRC) method and the WKJB method are used to derive an analytic formula for the surface currents on a two-dimensional perfectly conducting convex target. The

Manuscript received August 4, 1987; revised January 21, 1988. This work was supported in part by the NASA Lewis Research Center under Grant NAG 3-635 and in part by the National Science Foundation under Grants MCS-8300578 and DMS-870094.

T. G. Moore and A. Taflove are with the Department of Electrical Engineering and Computer Science, Technological Institute, Northwestern University, Evanston, IL 60208.

G. A. Kriegsmann is with the Department of Engineering Sciences and Applied Mathematics, Technological Institute, Northwestern University, Evanston, IL 60208.

IEEE Log Number 8821482.

currents are induced by an incident TE-polarized plane wave. The case of a circular cylinder is used to demonstrate the usefulness of the combined methods. It is shown that a two-term expansion yields good results for the surface currents and excellent results for the ensuing bistatic radar cross section.

#### I. INTRODUCTION

Recently, Kriegsmann *et al.* have introduced a new method for solving scattering problems for two-dimensional convex cylinders [1]. By applying a radiation boundary condition on the surface of the scatterer (OSRC) they obtained a simple analytic expression for the surface current when the incident wave was transverse magnetic (TM) polarized. When the incident wave was TE polarized, the method yielded an ordinary differential equation for the surface current. This equation contains variable coefficients which depend upon the geometry of the cylinder and the nature of the incident wave. In general, it cannot be solved exactly.

In this communication, we shall derive an approximate solution to this differential equation by using the WKBJ technique [2]. The motivation for such an approximation is twofold. First, it affords an accurate analytical approximation to the surface current without recourse to the numerical solution of a boundary value problem for arbitrary convex shapes. Secondly, and perhaps more importantly, a recent work by Jones [3] suggests that the approximate "surface current" for a three-dimensional convex acoustic target (hard) satisfies a second-order partial differential equation on the target's surface. We believe that a similar situation will occur when the OSRC method is extended to handle three-dimensional electromagnetic scattering problems. It seems plausible that the method presented herein could be extended to handle such situations.

The remainder of this work is organized in three additional sections. In Section II the scattering problem is formulated, and the OSRC method is used to derive an ordinary differential equation for the surface current. An approximate solution to this equation is deduced by the WKBJ method in Section III. Finally, in Section IV the results for a circular cylinder are presented.

#### II. FORMULATION

We shall consider a transverse electric plane wave illuminating a two-dimensional perfectly conducting convex cylinder. The incident wave, propagating at an angle  $\alpha$  with respect to the  $-x$  axis, is given by

$$\vec{H}_{\text{inc}} = U_{\text{inc}} e^{-j\omega t} \hat{z} \quad U_{\text{inc}} = e^{jk(x \cos \alpha - y \sin \alpha)} \quad (1)$$

where the unit vector  $\hat{z}$  is parallel to the axis of the cylinder. The parameter  $\omega$  is the frequency of the incident wave,  $k = \omega a/c$ ,  $c$  is the speed of light in free space, and  $a$  is a characteristic dimension of the cylinder's cross section. The variables  $x$  and  $y$  are the corresponding dimensionless Cartesian coordinates in the plane orthogonal to  $\hat{z}$ . They are scaled with respect to the length  $a$ .

The scattered magnetic field  $\vec{H}_s$  is given by

$$\vec{H}_s(\vec{x}) = U(\vec{x}) e^{-j\omega t} \hat{z} \quad (2a)$$

$$U(\vec{x}) = \int_C J(\vec{x}) \frac{\partial G}{\partial \nu'}(\vec{x}, \vec{x}') ds' \quad (2b)$$

where  $C$  represents the boundary of the cylinder's cross section,  $\partial/\partial \nu'$  denotes an outward normal derivative on  $C$ , and  $G$  is the free-space Green's function given by

$$G(\vec{x}|\vec{x}') = \frac{j}{4} H_0^{(1)}(kR) \quad (2c)$$